

Supplementary Information

Incorporating electron-deficient Cu nanoparticles in photoactive Zr-MOFs for highly efficient amine oxidative coupling with H₂O₂ photosynthesis

Leixin Hou,^{a,b*} Ziyan Li,^{a,b} Congfa Bian,^{a,b} Mi Zhang,^{a,b} Daofu Liu,^{a,b} Mai Xu^{a,b} and Huilin Huang^{c*}

^aSchool of Chemistry and Materials Engineering, Huainan Normal University, Huainan, Anhui, 232000, P. R. China

^b Anhui Engineering Research Center for Photoelectrocatalytic Electrode Materials, School of Chemistry and Material Engineering, Huainan Normal University, Huainan, Anhui, 232000, P. R. China

^cSchool of Chemical and Printing Dyeing Engineering, Henan University of Engineering, Zhengzhou, 451191, P. R. China

Corresponding Authors

* E-mail: houleixin@hnnu.edu.cn, huanghuilin321@126.com

Contents

1. Characterization of Photocatalysts
2. Visible-light Photocatalytic Oxidation Mediated by Zr-TPBD-Cu
3. References

1. Characterization of Photocatalysts

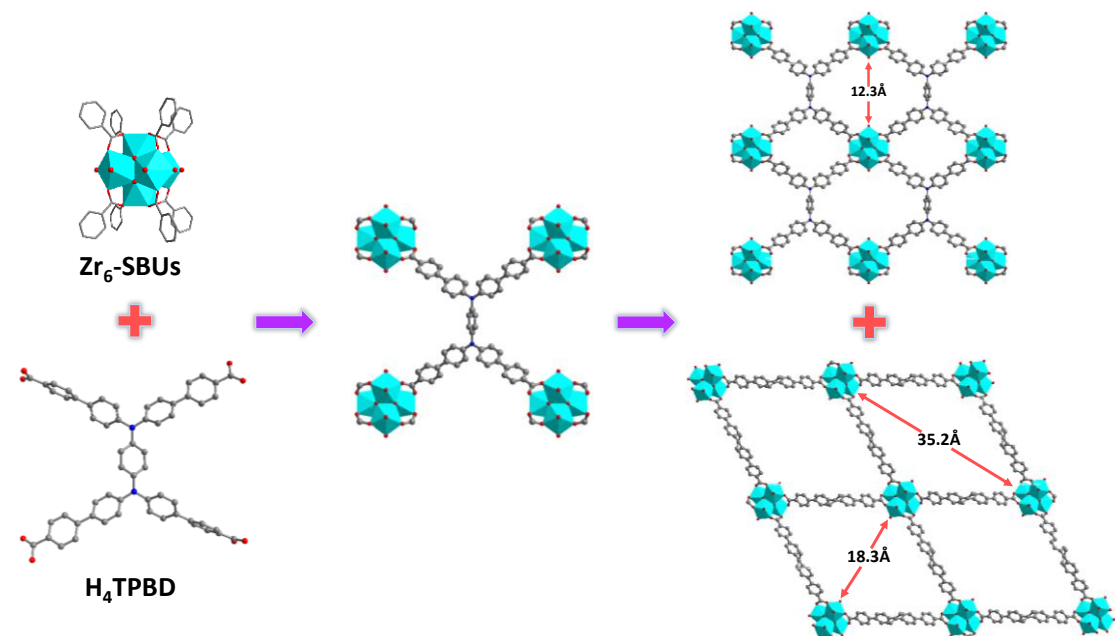


Figure S1. 3D framework of Zr-TPBD with Zr_6 -SBUs and H_4TPBD ligand. Hydrogen atoms and solvent molecules are omitted for clarity. Turquoise, Zr; red, O; gray, C; blue, N.

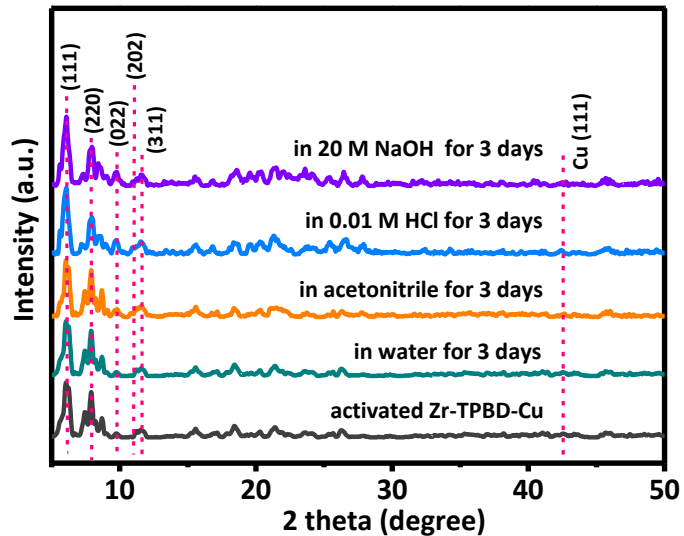


Figure S2. PXRD patterns of Zr-TPBD-Cu in different solvents.

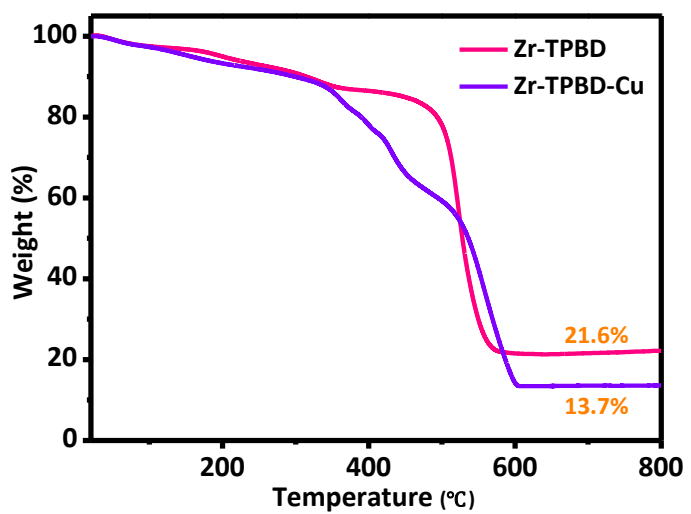


Figure S3. TGA curves of Zr-TPBD and Zr-TPBD-Cu samples.

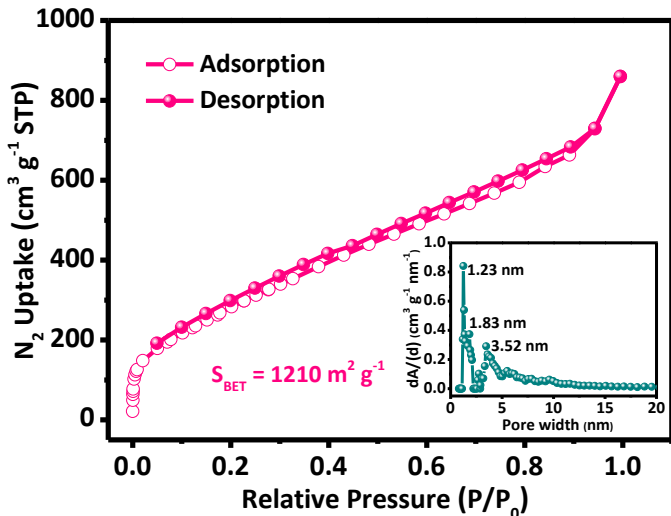


Figure S4. N_2 adsorption-desorption isotherms of Zr-TPBD (Insets: the pore size distributions). As shown in Figure 1c and S4, both Zr-TPBD nad Zr-TPBD-Cu samples exhibited unsaturated uptake at the point of $P/P_0 = 1$, which were attributed to the existence of the mixed micropore-mesoporous system in both materials. As a proof of concept, it is widely known that porous materials with a mixed micropore (1.23 nm and 1.83 nm) and mesoporous (3.52 nm) system may exhibit a superimposed effect of multi-layer adsorption and capillary coagulation in the high-pressure area, resulting in the adsorption curve not reaching a stable platform.

Dye Uptake Method: Before the dye uptake experiments, Zr-TPBD and Zr-TPBD-Cu were firstly washed with acetone three times for guest molecular exchange. Then, the Zr-TPBD and Zr-TPBD-Cu were soaked in a CH₃CN solution of Esoin Y on oscillator overnight at room temperature. The resulting MOFs were washed with CH₃CN solution thoroughly to remove the residual dye from the MOFs surfaces until the solution become colourless, and then dried under a stream of air. The dried-out MOFs were dissociated by 2mL concentrated hydrochloric acid, and the solution was diluted to 3mL CH₃CN. The absorption experiments were performed on a UV-vis spectroscopy. The concentration of Esoin Y dye was determined by comparing UV-vis absorption with the standard curve (Figure S5).

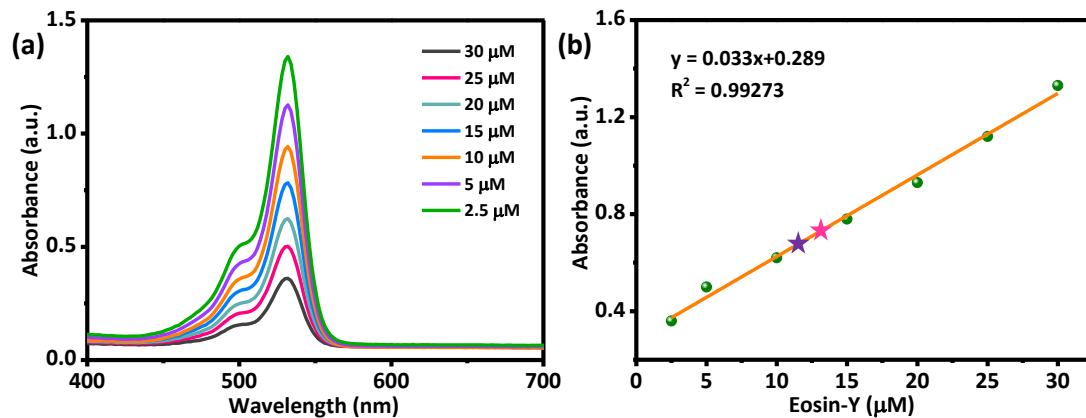


Figure S5. (a) UV-Vis spectra of Eosin Y in CH₃CN at different concentrations. (b) Plots of the absorbance of Eosin Y at 531 nm as a function of its concentration, and the absorbance of digested Zr-TPBD (pink asterisk) and Zr-TPBD-Cu (violet asterisk) in CH₃CN.

Table S1. Elemental analysis of Zr-TPBD-Cu sample.

Sample	Atomic contents				
	C (wt %)	N (wt %)	O (wt %)	Zr (wt %)	Cu (wt %)
Zr-TPBD-Cu	50.5	2.15	20.3	19.5	5.1

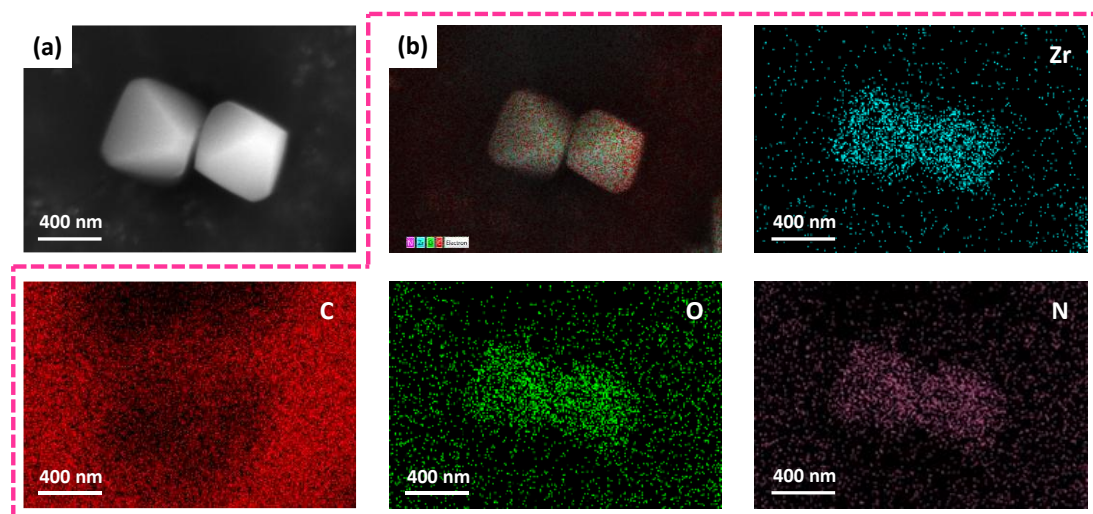


Figure S6. (a) SEM and (b) EDS mapping images of Zr-TPBD.

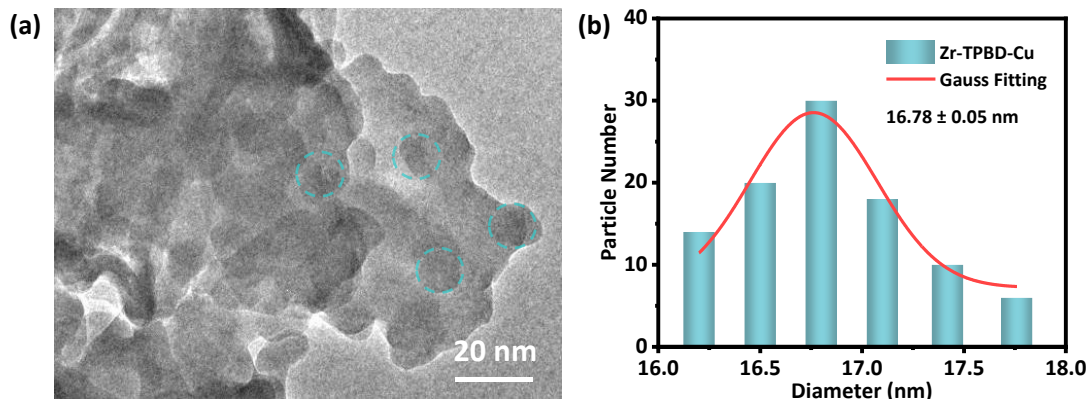


Figure S7. (a) HRTEM image of Zr-TPBD-Cu. (b) The corresponding histogram of nanomicelle sizes obtained from TEM image.

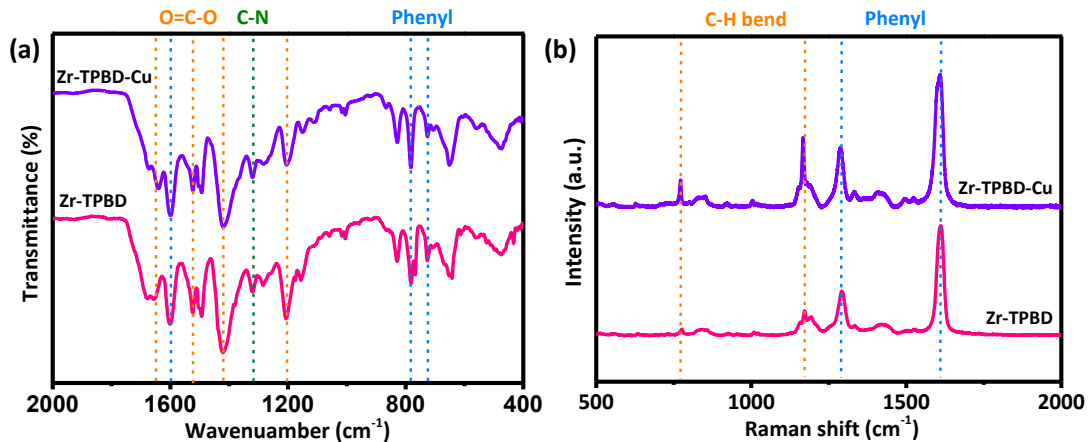


Figure S8. (a) The Diffuse Reflectance FT-IR and (b) the laser Raman confocal microspectrometry of Zr-TPBD and Zr-TPBD-Cu. Fourier transform infrared (FT-IR) spectra were collected in the range of 400-3500 cm^{-1} as KBr pellets on Thermo Fisher-6700. Raman spectra were collected on a Lab Raman HR Evolution at excitation wavelength of 633 nm in a scan range from 500 to 2000 cm^{-1} on powdered samples on air.

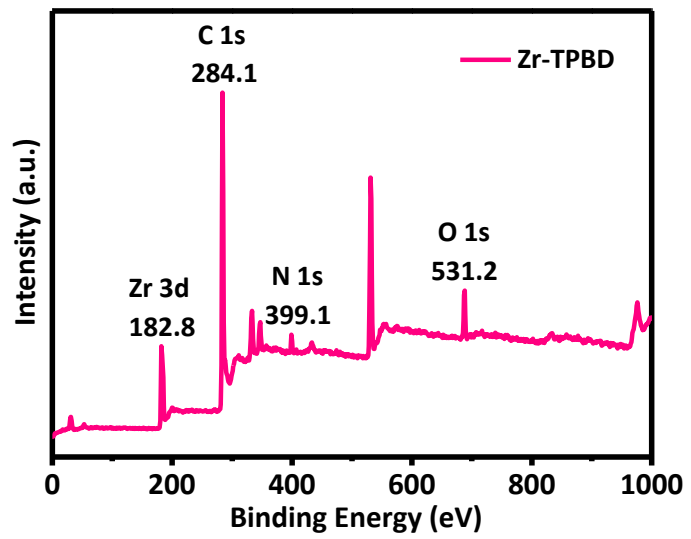


Figure S9. XPS full-scale spectrum of the as-prepared Zr-TPBD.

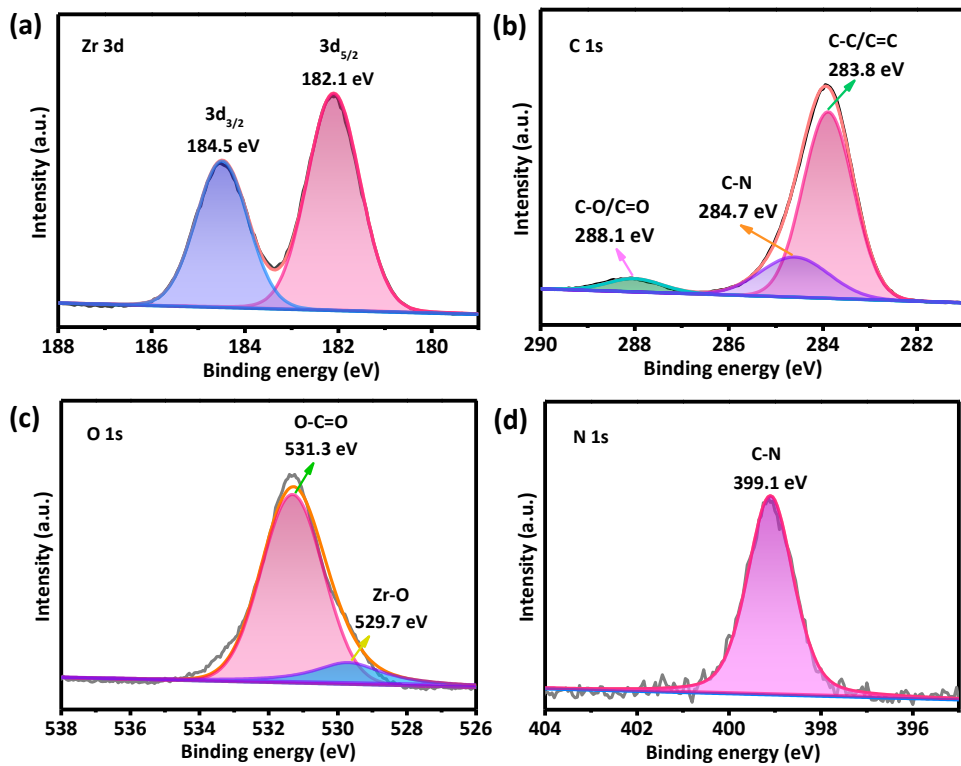


Figure S10. (a) Zr3d spectrum, (b) C1s spectrum, (c) O1s spectrum and (d) N1s spectrum of Zr-TPBD.

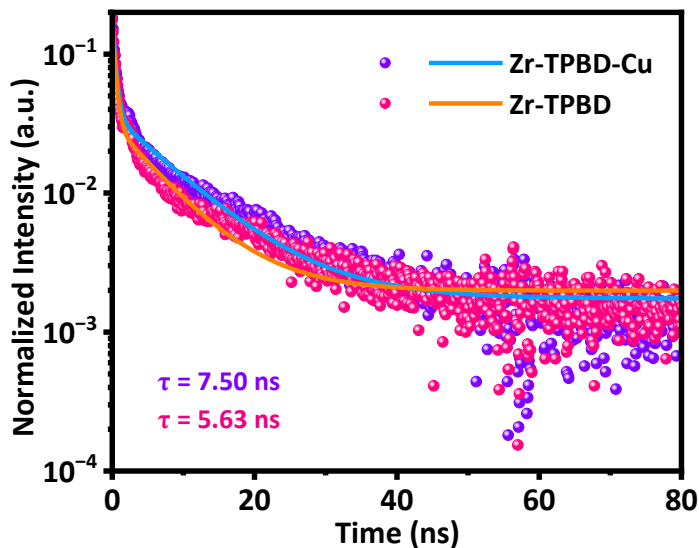


Figure S11. Transient fluorescence lifetime spectra analyses and fitting results of Zr-TPBD and Zr-TPBD-Cu.

Table S2. Average fluorescence lifetime fitting of Zr-TPBD and Zr-TPBD-Cu.

Sample	A_1	τ_1	A_2	τ_2
Zr-TPBD	0.14118	0.44453	0.02964	7.15898
Zr-TPBD-Cu	0.14089	0.46952	0.0351	8.94261

The decay curves of Zr-TPBD and Zr-TPBD-Cu were fitted based on the equation: $y = y_0 + A_1 \exp(-t/\tau_1) + A_2 \exp(-t/\tau_2)$. The average lifetime was calculated by using the equation: $\tau = (A_1 \tau_1^2 + A_2 \tau_2^2) / (A_1 \tau_1 + A_2 \tau_2)$.

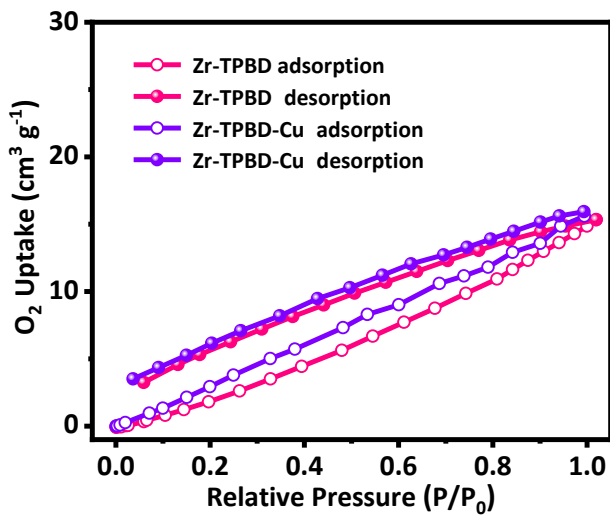


Figure S12. Adsorption-desorption curves of O_2 on Zr-TPBD and Zr-TPBD-Cu.

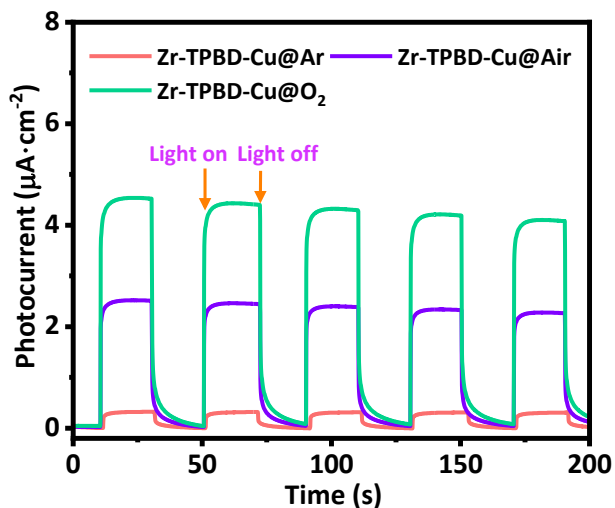


Figure S13. Transient photocurrents of Zr-TPBD-Cu sample recorded in air, O₂ and Ar atmospheres.

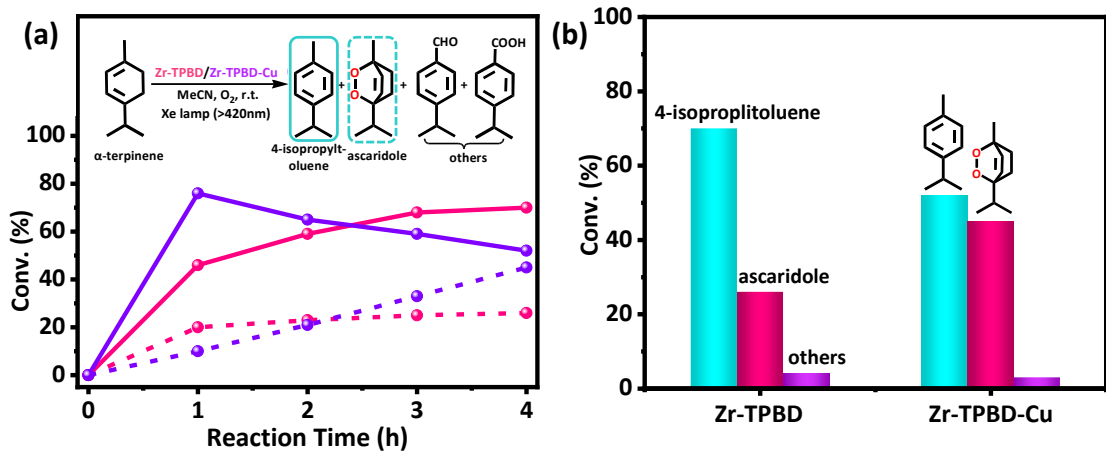


Figure S14. (e) Kinetic profiles of the oxidation of α -terpinene to 4-isopropyltoluene (solid line) and ascaridole (dotted line) catalysed by Zr-TPBD (pink) and Zr-TPBD-Cu (violet) under 300 W Xe lamp ($\lambda > 420\text{ nm}$) illumination. (f) Conversion of aterpinene into 4-isopropyltoluene, ascaridole, and others catalysed by both Zr-MOFs. As shown in Fig. S14, under Xe lamp ($\lambda > 420\text{ nm}$) irradiation, the conversion rate of α -terpinene oxidation within 1 h using Zr-TPBD-Cu as photocatalyst can reach 100 % with a selectivity of 76% for associated-•O₂⁻ aromatic product, indicating that the primary ROS was identified as •O₂⁻ during the initial catalytic stages.

2. Visible-light Photocatalytic Oxidation Mediated by Zr-TPBD-Cu

Table S3. Comparison of photocatalytic H₂O₂ production rates of Zr-TPBD-Cu and other recently reported photocatalysts.

Catalysts	Reaction pathway	H ₂ O ₂ yield ($\mu\text{mol}\cdot\text{g}^{-1}\cdot\text{h}^{-1}$)	AQY (%)	Reference
Zr-TPBD-Cu	Benzylamine oxidation, ORR	73500	13.1	This work
Zr-TPBD		16300	/	
Co ₁₄ (L-CH ₃) ₂₄	WOR, ORR	146.6	/	S1
BTDB-CN _{0.2}	ORR	1920	2.99	S2
Ca(II)@ACG	ORR	1021.5	/	S3
ZrS ₃ NBs	ORR	1560	11.4	S4
NMT400	ORR	1695.3	2.6	S5
BBTz	ORR	7274	7.14	S6
N-AT/PTCA	ORR	63520	15.9	S7
D-A CNP-s	ORR	32000	/	S8
TPC-3D	ORR	9991	30.9	S9
Nv-C=N-CN	ORR	3093	1.8	S10
NiSAPs-PuCN	ORR	342.2	10.9	S11
UCN-DTDA	ORR	7300	/	S12
CN-NH ₄ -NaK	ORR	16675	28.4	S13
CN-KI ₃ -KI-MV	ORR	46400	27.56	S14
2L-mCN/F-Naf	ORR	5380	/	S15
CNNT-Al	WOR	1410.2	7.9	S16
Zn-MOF(lc)/400	ORR	4780	/	S17
Au-TFPT	ORR, WOR	51987	1.8	S18

CuBr-dptz	ORR	1874	0.4	S19
EFB-MOF	ORR	1676	/	S20
JNM-25	ORR, OER	17476	4.72	S21
UiO/IKCN	ORR	13300	10.28	S22
C ₃ N ₄ -Zn-N(C)	ORR	7800	26.8	S23
TAPD-(Me) ₂ COF	ORR	234.52	/	S24
COF-N32	ORR	605	6.2	S25
Daz COFs	ORR	7327	11.9	S26
TTH-CTP	ORR	23700	9.6	S27
EO-COF	ORR	2675	6.57	S28
TFPA-TAPT-COF-Q	ORR	11831.6	/	S29
D-A COF-2	ORR, WOR	6930	2.5	S30
PTH-S-COF	ORR, OER	13565	/	S31

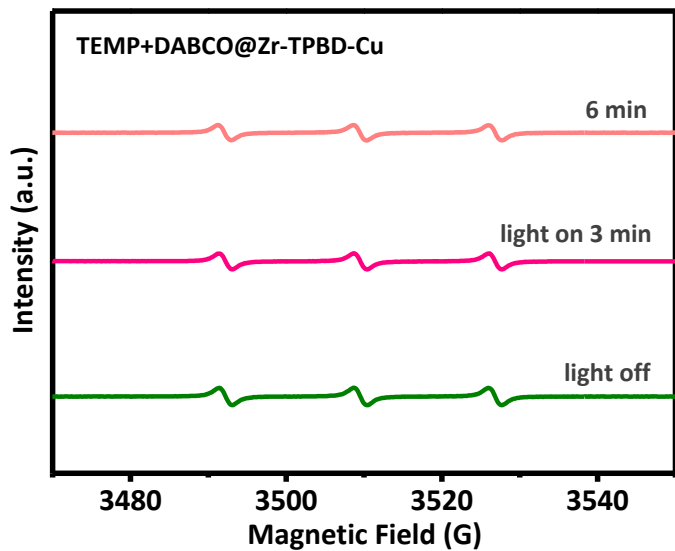


Figure S15. EPR detection of ${}^1\text{O}_2$ species trapped by TEMP in presence of DABCO quencher over Zr-TPBD-Cu under light irradiation.

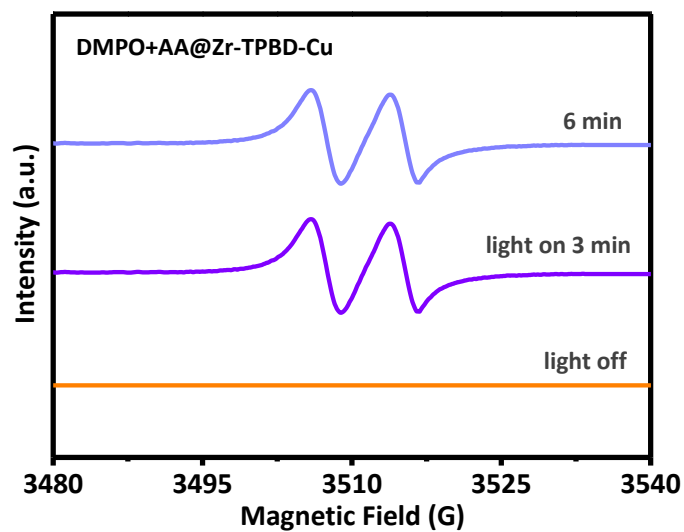


Figure S16. EPR detection of $\text{O}_2^{\cdot-}$ species trapped by DMPO in presence of ascorbic acid (AA) quencher over Zr-TPBD-Cu under light irradiation.

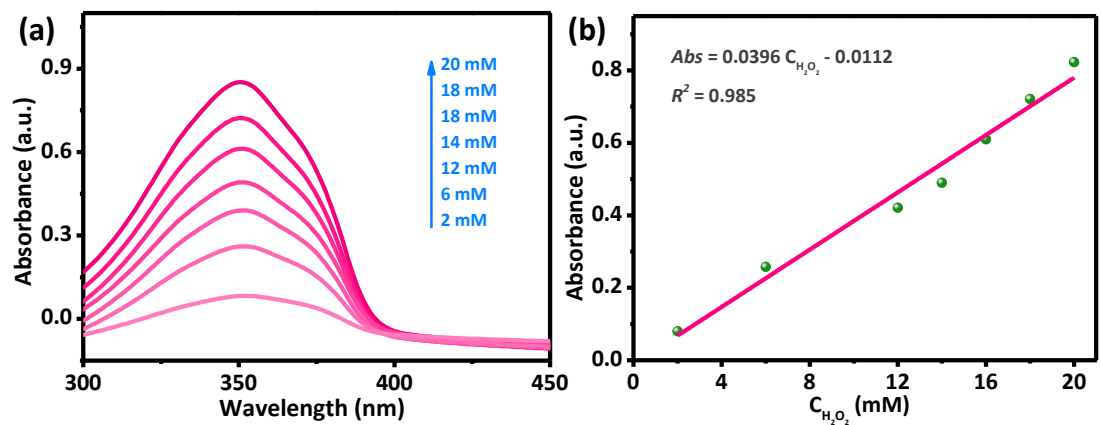


Figure S17. (a) UV-Vis absorption spectra of different H_2O_2 concentrations by iodimetry.
 (b) The standard linear relationship between the absorption and H_2O_2 concentrations.

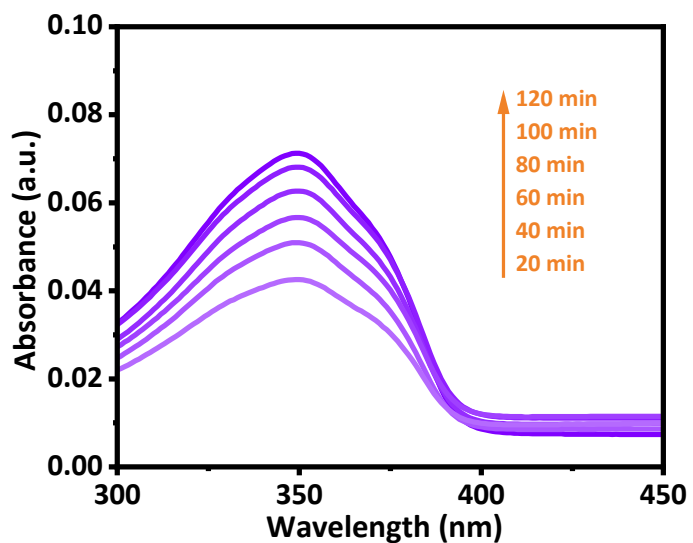


Figure S18. Time-dependent UV-vis absorption spectra of generated H_2O_2 by iodimetry in H_2O_2 photosynthesis coupled with BA oxidative coupling reaction.

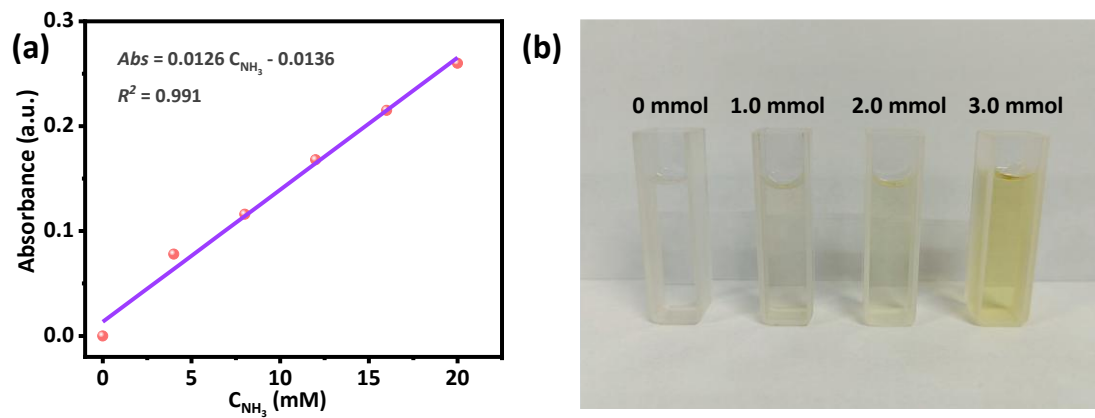


Figure S19. (a) Linear fitting of standard NH_3 concentrations, (b) optical photograph of the solution containing yellow complex formed by Nessler reagent and NH_3 when photocatalytic conversion of different amounts of benzylamine by Zr-TPBD-Cu. NH_3 was produced at the final reaction step of benzylamine coupling, which was verified by Nessler reagent colorimetry.

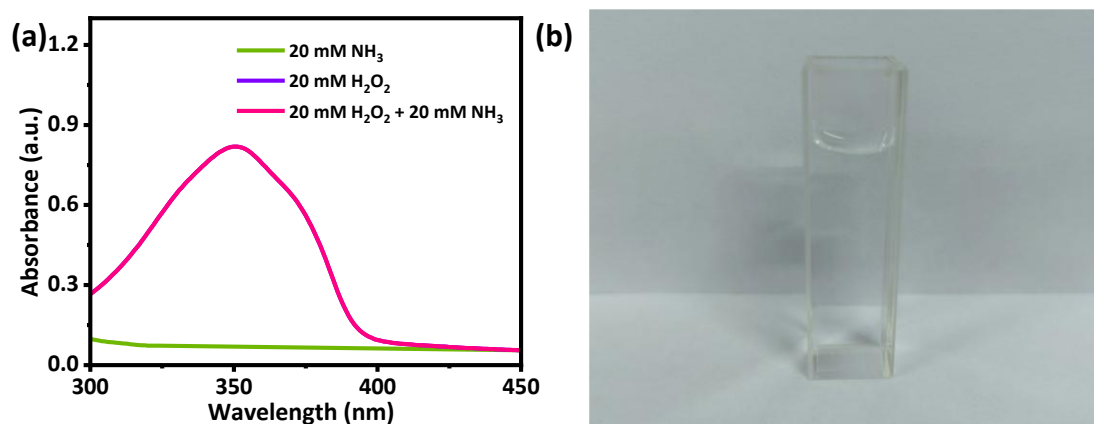


Figure S20. (a) UV-Vis absorption spectra of 20 mM NH₃, 20 mM H₂O₂ and 20 mM H₂O₂ + 20 mM NH₃ in iodimetry, (b) optical photograph of the solution containing 20 mM NH₃ and iodine reagent. The interference from NH₃ in determining the H₂O₂ yield was also excluded as no chromogenic reaction occurred to NH₃ in iodimetry method.

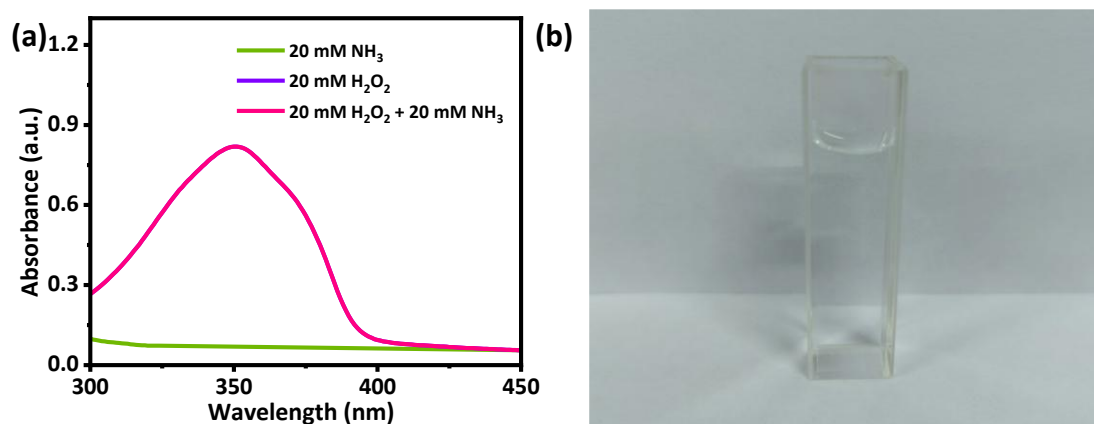


Figure S21. (a) UV-Vis absorption spectra of 20 mM NH₃, 20 mM H₂O₂ and 20 mM H₂O₂ + 20 mM NH₃ in iodimetry, (b) optical photograph of the solution containing 20 mM NH₃ and iodine reagent. The interference from NH₃ in determining the H₂O₂ yield was also excluded as no chromogenic reaction occurred to NH₃ in iodimetry method.

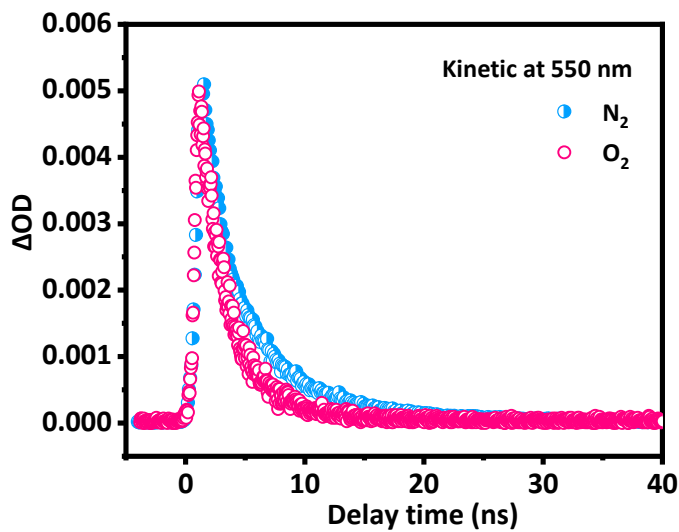


Figure S22. The ns-TA spectra decay curve monitored at 550 nm for Zr-TPBD-Cu in N_2 and O_2 .

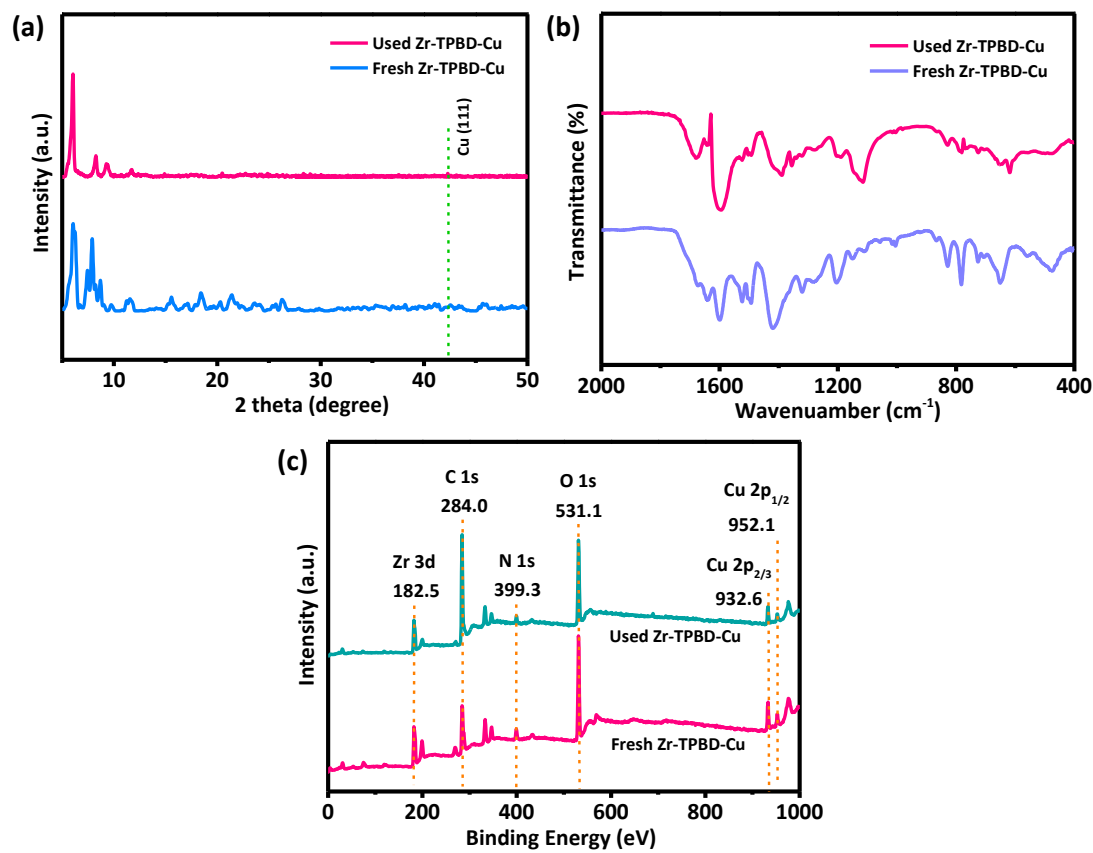
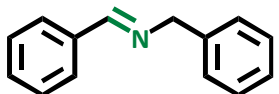


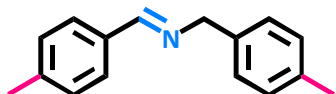
Figure S23. (a) PXRD patterns, (b) FTIR spectra and (c) XPS survey spectra of fresh and used Zr-TPBD-Cu.

N-benzyl-1-phenylmethanimine



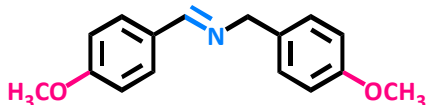
¹H NMR (400 MHz, CDCl₃): 4.86 (s, 2H), 7.31-7.45 (m, 8H), 7.81-7.89 (m, 2H), 8.29 (s, 1H)

N-(4-methylbenzyl)-1-(*p*-tolyl)methanimine



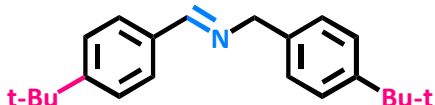
¹H NMR (400 MHz, CDCl₃): 2.34 (s, 3H), 2.38 (s, 3H), 4.76 (s, 2H), 7.14-7.24 (m, 6H), 7.67 (d, 2H, *J* = 8.0 Hz), 8.34 (s, 1H).

N-(4-methoxybenzyl)-1-(4-methoxyphenyl)methanimine



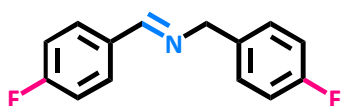
¹H NMR (400 MHz, CDCl₃): 3.74 (s, 3H), 3.81 (s, 3H), 4.67 (s, 2H), 6.91 (d, 2H, *J* = 8.4 Hz), 7.02 (d, 2H, *J* = 8.8 Hz), 7.26 (d, 2H, *J* = 8.8 Hz), 7.73 (d, 2H, *J* = 8.8 Hz), 8.36 (s, 1H).

N-(4-butylbenzyl)-1-(4-butylphenyl)methanimine



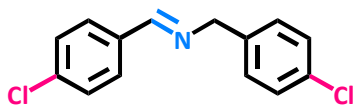
¹H NMR (400 MHz, CDCl₃): 0.97-1.01 (m, 6H), 1.37-1.47 (m, 4H), 1.61-1.71 (m, 4H), 2.64-2.71 (m, 4H), 4.83 (s, 2H), 7.21 (d, 2H, *J* = 8.0 Hz), 7.26-7.31 (m, 4H), 7.75 (d, 2H, *J* = 8.4 Hz), 8.41 (s, 1H).

N-(4-fluorobenzyl)-1-(4-fluorophenyl)methanimine



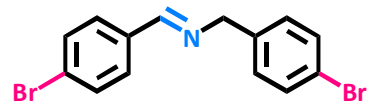
¹H NMR (400 MHz, CDCl₃): 4.73 (s, 2H), 7.14 (dd, 2H, *J* = 12.4, 5.4 Hz), 7.26 (t, 2H, *J* = 8.8 Hz), 7.35 (dd, 2H, *J* = 8.5, 5.7 Hz), 7.79-7.91 (m, 2H), 8.45 (s, 1H).

N-(4-chlorobenzyl)-1-(4-chlorophenyl)methanimine



¹H NMR (400 MHz, CDCl₃): 4.75 (s, 2H), 7.33-7.40 (m, 4H), 7.50 (d, 2H, *J* = 8.6 Hz), 7.79 (d, 2H, *J* = 8.4 Hz), 8.48 (s, 1H).

N-(4-bromobenzyl)-1-(4-bromophenyl)methanimine



¹H NMR (400 MHz, CDCl₃): 4.72 (s, 2H), 7.29 (d, 2H, *J* = 8.4 Hz), 7.52 (d, 2H, *J* = 8.5 Hz), 7.65 (d, 2H, *J* = 8.8 Hz), 7.72 (d, 2H, *J* = 8.4 Hz), 8.47 (s, 1H).

3. References

- S1. J. N. Lu, J. J. Liu, L. Z. Dong, J. M. Lin, F. Yu, J. Liu and Y. Q. Lan, *Angew. Chem. Int. Ed.*, 2023, **62**, e202308505.
- S2. J. Z. Cheng, W. Wang, J. J. Zhang, S. J. Wan, B. Cheng, J. G. Yu and S. W. Cao, *Angew. Chem. Int. Ed.*, 2024, **63**, e202406310.
- S3. C. He, J. Y. Lei, X. Li, Z. Y. Shen, L. Z. Wang and J. L. Zhang, *Angew. Chem. Int. Ed.*, 2024, **63**, e202406143.
- S4. Z. L. Tian, C. Han, Y. Zhao, W. R. Dai, X. Lian, Y. N. Wang, Y. Zheng, Y. Shi, X. Pan, Z. C. Huang, H. X. Li and W. Chen, *Nat. Commun.*, 2021, **12**, 2039.
- S5. C. Yang, S. J. Wan, B. C. Zhu, J. G. Yu and S. W. Cao, *Angew. Chem. Int. Ed.*, 2022, **61**, e202208438.
- S6. J. Z. Cheng, S. J. Wan and S. W. Cao, *Angew. Chem. Int. Ed.*, 2023, **62**, e202310476.
- S7. R. Ji, Y. M. Dong, X. Y. Sun, C. S. Pan, Y. F. Yang, H. Zhao and Y. F. Zhu, *Appl. Catal. B Environ. Energ.*, 2024, **349**, 123884.
- S8. H. F. Yang, C. Li, T. Liu, T. Fellowes, S. Y. Chong , L. Catalano, M. Bahri , W. W. Zhang, Y. J. Xu, L. J. Liu , W. Zhao, A. M. Gardner, R. Clowes, N. D. Browning, X. B. Li , A. J. Cowan and A. I. Cooper, *Nat. Nanotechnol.*, 2023, **18**, 307–315.
- S9. Y. Y. Huang, M. H. Shen, H. J. Yan, Y. G. He, J. Q. Xu, F. Zhu, X. Yang, Y. X. Ye and G. F. Ouyang, *Nat. Commun.*, 2024, **15**, 5406.
- S10. X. Zhang, P. J. Ma, C. Wang, L. Y. Gan, X. J. Chen, P. Zhang, Y. Wang, H. Li, L. H. Wang, X. Y. Zhou and K. Zheng, *Energ. Environ. Sci.*, 2022, **15**, 830–842.
- S11. X. Zhang, H. Su, P. X. Cui, Y. Y. Cao, Z. Y. Teng, Q. T. Zhang, Y. Wang, Y. B. Feng, R. Feng, J. X. Hou, X. Y. Zhou, P. J. Ma, H. W. Hu, K. W. Wang, C. Wang, L. Y. Gan, Y. X. Zhao, Q. H. Liu, T. R. Zhang and K. Zheng, *Nat. Commun.*, 2023, **14**, 7115.
- S12. P. Z. Sha, L. Huang, J. Zhao, Z. H. Wu, Q. F. Wang, L. B. Li, D. L. Bu and S. M. Huang, *ACS Catal.*, 2023, **13**, 10474–10486.
- S13. F. T. He, Y. M. Lu, Y. Z. Wu, S. L. Wang, Y. Zhang, P. Dong, Y. Q. Wang, C. C. Zhao, S. J. Wang, J. Q. Zhang and S. B. Wang, *Adv. Mater.*, 2024, **36**, 2307490.

- S14. C. W. Bai, L. L. Liu, J. J. Chen, F. Chen, Z. Q. Zhang, Y. J. Sun, X. J. Chen, Q. Yang and H. Q. Yu, *Nat. Commun.*, 2024, **15**, 4718.
- S15. Y. X. Li, Z. H. Pei, D. Y. Luan and X. W. D. Lou, *J. Am. Chem. Soc.*, 2024, **146**, 3343–3351.
- S16. H. Tan, P. Zhou, M. X. Liu, Y. Gu, W. X. Chen, H. Y. Guo, J. K. Zhang, K. Yin, Y. Zhou, C. S. Shang, Q. H. Zhang, L. Gu, N. Zhang, J. Y. Ma, Z. F. Zheng, M. C. Luo and S. J. Guo, *J. Am. Chem. Soc.*, 2024, **146**, 31950–31960.
- S17. Y. X. Li, Y. Guo, D. Y. Luan, X. J. Gu and X. W. D. Lou, *Angew. Chem. Int. Ed.*, 2023, **62**, e202310847.
- S18. P. Wu, F. M. Du, Q. Xue, H. X. Li, M. C. Fu, X. K. Zhou and F. Wang, *Adv. Funct. Mater.*, 2025, **35**, 2420941.
- S19. J. P. Zhang, H. Lei, Z. J. Li, F. L. Jiang, L. Chen and M. C. Hong, *Angew. Chem. Int. Ed.*, 2024, **63**, e202316998.
- S20. J. Y. Choi, B. Check, X. Y. Fang, S. Blum, H. T. B. Pham, K. Tayman and J. Park, *J. Am. Chem. Soc.*, 2024, **146**, 11319–11327.
- S21. Y. Y. Tang, X. Luo, R. Q. Xia, J. Luo, S. K. Peng, Z. N. Liu, Q. Gao, M. Xie, R. J. Wei, G. H. Ning and D. Li, *Angew. Chem. Int. Ed.*, 2024, **63**, e202408186.
- S22. X. Z. Lu, Z. W. Chen, Z. F. Hu, F. Y. Liu, Z. H. Zuo, Z. X. Gao, H. G. Zhang, Y. C. Zhu, R. Z. Liu, Y. G. Yin, Y. Cai, D. L. Ma and Q. Z. Zhang, *Adv. Energy Mater.*, 2024, **14**, 2401873.
- S23. W. K. Wang, R. Liu, J. J. Zhang, T. T. Kong, L. L. Wang, X. H. Yu, X. M. Ji, Q. Q. Liu, R. Long, Z. Lu and Y. J. Xiong, *Angew. Chem. Int. Ed.*, 2024, **63**, e202415800.
- S24. C. Krishnaraj, H. S. Jena, L. Bourda, A. Laemont, P. Pachfule, J. Roeser, C. V. Chandran, S. Borgmans, S. M. J. Rogge, K. Leus, C. V. Stevens, J. A. Martens, V. V. Speybroeck, E. Breynaert, A. Thomas and P. V. D. Voort, *J. Am. Chem. Soc.*, 2020, **142**, 20107–20116.
- S25. F. Y. Liu, P. Zhou, Y. H. Hou, H. Tan, Y. Liang, J. L. Liang, Q. Zhang , S. J. Guo, M. P. Tong and J. R. Ni, *Nat. Commun.*, 2023, **14**, 4344.
- S26. Q. B. Liao, Q. N. Sun, H. C. Xu, Y. D. Wang, Y. Xu, Z. Y. Li, J. W. Hu, D. Wang, H. J. Li and K. Xi, *Angew. Chem. Int. Ed.*, 2023, **62**, e202310556.

- S27. S. D. Wang, Z. P. Xie, D. Zhu, S. Fu, Y. S. Wu, H. L. Yu, C. Y. Lu, P. K. Zhou, M. Bonn, H. I. Wang, Q. Liao, H. Xu, X. Chen and C. Gu, *Nat. Commun.*, 2023, **14**, 6891.
- S28. P. J. Li, F. Y. Ge, Y. Yang, T. Y. Wang, X. Y. Zhang, K. Zhang and J. Y. Shen, *Angew. Chem. Int. Ed.*, 2024, **63**, e202319885.
- S29. J. R. Wang, K. P. Song, T. X. Luan, K. Cheng, Q. R. Wang, Y. Wang, W. W. Yu, P. Z. Li and Y. L. Zhao, *Nat. Commun.*, 2024, **15**, 1267.
- S30. Y. H. Xie, F. Y. Mao, Q. Y. Rong, X. L. Liu, M. J. Hao, Z. S. Chen, H. Yang, G. I. N. Waterhouse, S. Q. Ma and X. K. Wang, *Adv. Funct. Mater.*, 2024, **34**, 2411077.
- S31. Y. Y. Peng, L. W. Yuan, K. K. Liu, Z. J. Guan, S. B. Jin and Y. Fang, *Angew. Chem. Int. Ed.*, 2024, **63**, e202423055.